iScience

CellPress
OPEN ACCESS

Article

Glioblastoma extracellular vesicles modulate immune PD-L1 expression in accessory macrophages upon radiotherapy

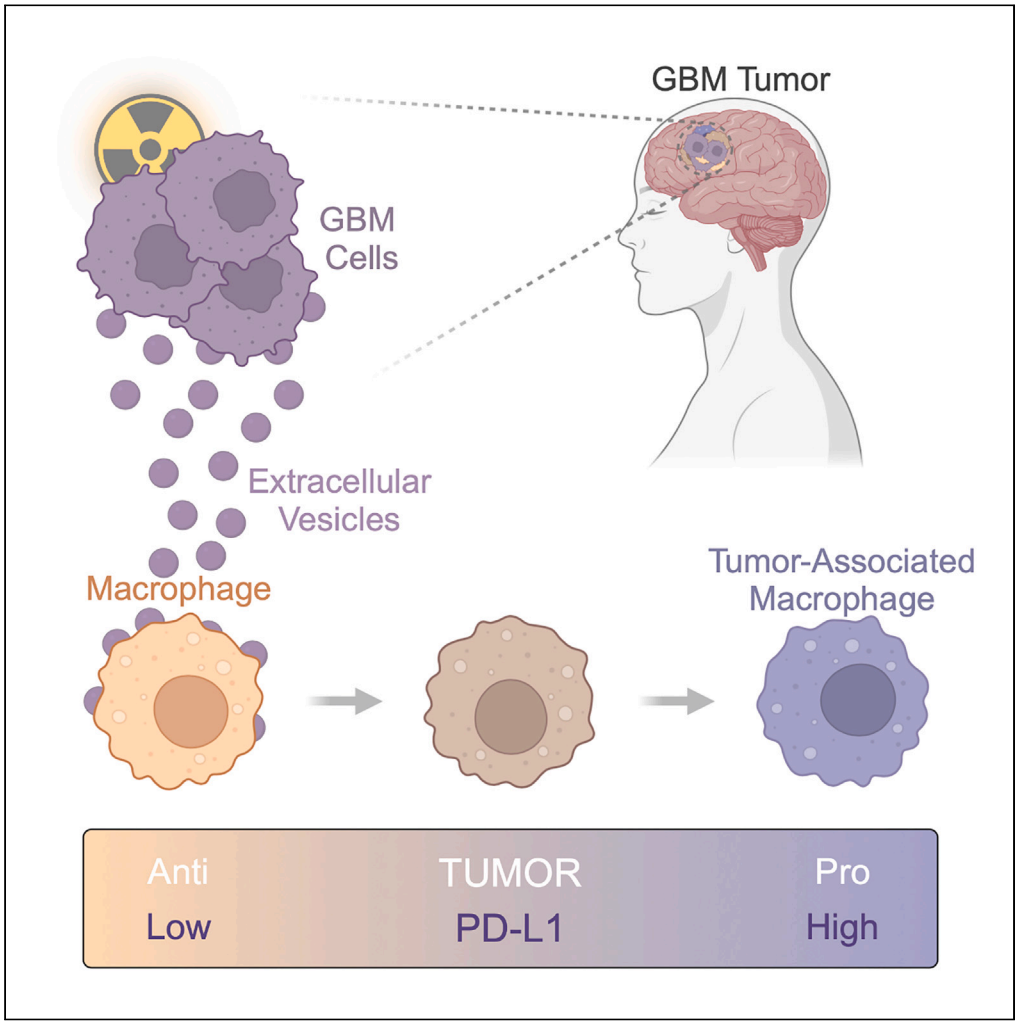

Markus W. Schweiger, Zohreh Amoozgar, Pierre Repiton, ..., Wilhelm Haas, Koen Breyne, Bakhos A. Tannous

kbreyne@mgh.harvard.edu (K.B.)
bakhos.tannous@astrazeneca.com (B.A.T.)

Highlights

Radiation increases the expression of immune-suppressive markers on GBM cells

Macrophages in the GBM microenvironment take up tumor-derived signals through EVs

GBM EVs enhance phagocytosis and PD-L1 expression in recipient macrophages

Schweiger et al., iScience 27, 108807
February 16, 2024
https://doi.org/10.1016/j.isci.2024.108807

iScience

CellPress
OPEN ACCESS

Article

Glioblastoma extracellular vesicles modulate immune PD-L1 expression in accessory macrophages upon radiotherapy

Markus W. Schweiger,[1,2,3,4] Zohreh Amoozgar,[5] Pierre Repiton,[1,2,6] Robert Morris,[7] Semer Maksoud,[1,2] Michael Hla,[1,2] Eric Zaniewski,[7] David P. Noske,[3,4] Wilhelm Haas,[7,8] Koen Breyne,[1,2,10,*] and Bakhos A. Tannous[1,2,9,*]

SUMMARY

Glioblastoma (GBM) is the most aggressive brain tumor, presenting major challenges due to limited treatment options. Standard care includes radiation therapy (RT) to curb tumor growth and alleviate symptoms, but its impact on GBM is limited. In this study, we investigated the effect of RT on immune suppression and whether extracellular vesicles (EVs) originating from GBM and taken up by the tumor microenvironment (TME) contribute to the induced therapeutic resistance.

We observed that (1) ionizing radiation increases immune-suppressive markers on GBM cells, (2) macrophages exacerbate immune suppression in the TME by increasing PD-L1 in response to EVs derived from GBM cells which is further modulated by RT, and (3) RT increases CD206-positive macrophages which have the most potential in inducing a pro-oncogenic environment due to their increased uptake of tumor-derived EVs.

In conclusion, RT affects GBM resistance by immuno-modulating EVs taken up by myeloid cells in the TME.

INTRODUCTION

Glioblastoma (GBM) represents the most aggressive and lethal form of brain cancer, with only 6.9% of patients surviving five years post-diagnosis.[1] Radiation therapy (RT), in combination with temozolomide and surgical resection, is part of the standard treatment regimen and has been shown to be a key factor in improving survival.[1–4] However, despite a multimodal treatment approach, the prognosis remains dismal. The limited efficacy of RT against GBM has been attributed to pro-oncogenic resistance signaling in cancer cells and its tumor microenvironment (TME), which serves as a protective and immunosuppressive shield.[5–7] The latter resistance programming is mainly facilitated by tumor-associated macrophages and microglia (TAMs), which include both peripheral macrophages and brain-resident myeloid cells and can constitute up to 30%–50% of the tumor mass.[8,9]

Recent research has shed light on mechanisms that drive TAM-mediated resistance: it has been proposed that phagocytosis by myeloid cells can lead to the adoptive transfer of programmed death ligand 1 (PD-L1), further enhancing GBM immune evasion.[10,11] Additionally, GBM-derived extracellular vesicles (EVs) are gaining recognition as key factors in modulating the TME. They have been shown to be internalized by myeloid cells, thereby influencing their behavior and consequently promoting a pro-tumorigenic environment.[12–16]

Here, we investigated the impaired antitumor immunity induced by GBM in response to RT. We focus on the myeloid compartment of the TME that is susceptible to protumoral/reprogramming signals dictated by GBM cancer cells. Specifically, we focus on immune-suppressive triggers transferred by tumor-derived EVs when GBM cancer cells are stressed by ionizing radiation. We show that RT triggers increased levels of PD-L1 (an essential immune checkpoint protein[17]) and CD47 (a prominent "don't-eat-me signal"[18]) in different glioma models. Mainly CD206-positive myeloid cells perceive GBM cues and subsequently increase their PD-L1 expression independent from conventional phagocytosis-mediated PD-L1 transfer post-tumor-derived EV uptake. Concomitantly, we observed reprogramming of myeloid cell behavior,

[1]Department of Neurology, Massachusetts General Hospital, Harvard Medical School, Boston, MA 02129, USA
[2]Neuroscience Program, Harvard Medical School, Boston, MA 02129, USA
[3]Amsterdam UMC Location Vrije Universiteit Amsterdam, Department of Neurosurgery, 1081 HV Amsterdam, the Netherlands
[4]Cancer Center Amsterdam, Brain Tumor Center and Liquid Biopsy Center, 1081 HV Amsterdam, the Netherlands
[5]Department of Radiation Oncology, Edwin L. Steele Laboratories, Massachusetts General Hospital Cancer Center, Massachusetts General Hospital and Harvard Medical School, Boston, MA 02114, USA
[6]Section of Pharmaceutical Sciences, Institute of Pharmaceutical Sciences of Western Switzerland, University of Geneva, 1205 Geneva, Switzerland
[7]Massachusetts General Hospital Cancer Center, Boston, MA 02129, USA
[8]Department of Medicine, Harvard Medical School, Boston, MA 02129, USA
[9]Present address: Early Oncology R&D, ICC, AstraZeneca, Waltham, MA 02451, USA
[10]Lead contact
*Correspondence: kbreyne@mgh.harvard.edu (K.B.), bakhos.tannous@astrazeneca.com (B.A.T.)
https://doi.org/10.1016/j.isci.2024.108807

including altered cytokine secretion, enhanced phagocytosis, and increased PD-L1 expression in line with a switch toward a more immune-suppressive phenotype. Overall, our findings support that EVs serve as vectors to enhance the immune suppression program induction in the TME, thereby protecting GBM cancer cells stressed by RT.

RESULTS

Radiation therapy induces the expression of immune-suppressive markers on GBM cells

To assess the impact of RT on GBM, CT-2A mouse glioma cells were exposed to 5 Gray (Gy) ionizing radiation and analyzed 48 h later by proteomics. CT-2A cells were selected based on their potential to establish a murine glioma model after intracranial engraftment that resembles brain tumor stem cell growth[19,20] and recurrent GBM in patients.[21] Pathway analysis of proteomics data was analyzed based on a normalized enrichment score above 1.6 or below −1.6. Ionizing radiation increased immunomodulatory protein expression, including humoral, B cell, and adaptive immunity, while decreasing growth and development signaling (Figure 1A). We corroborated these results by exposing two murine glioma models, CT-2A and GL261, to ionizing radiation and analyzed the expression of genes encoding for well-described immune-suppressive markers (PD-L1, CD47, CD155, and CD112) on cancer cells[17,18,22,23] (Figure 1B). Interestingly, PD-L1 and CD47 levels increased in a dose-dependent manner in response to RT in both glioma models, while levels of CD155 and CD112 did not. TCGA survival analysis[24,25] revealed no significant survival benefit for GBM patients with either low PD-L1 or CD47 expression. However, in combination, high CD47 and PD-L1 levels are associated with poor survival for patients (Figure 1C).

To verify the observed RT-mediated effect *in vivo*, mCherry-expressing CT-2A cells were intracranially implanted into C57BL/6 mice, and 14 days later, mice heads were subjected to either a single dose of 5 Gy or five doses of fractionated 2 Gy ionizing radiation mimicking human treatment protocols[26,27] (Figure 1D - top). Single-cell suspensions were obtained from tumor-bearing hemispheres 20 days post-tumor implantation for flow cytometric analysis. Tumor cells were distinguished from immune cells in the TME based on mCherry and CD45 expression, respectively ($CD45^{NEG}mCherry^{POS}$) (Figure S1). Interestingly, both radiation regimens resulted in a significant ~1.5-fold elevation of surface-expressed PD-L1 levels on tumor cells (Figure 1D - bottom). CD47 display was less pronounced, with only significance after the 5 × 2 Gy radiation protocol. Collectively, these findings suggest that GBM tumors have immuno-suppressive potential, which can be further exacerbated by ionizing radiation.

The propensity of macrophages, over other cells in the GBM TME, to take up tumor-derived signals through EVs

The GBM TME is characterized by a heterogeneous population of immune cells, both resident and recruited from the blood.[8] We aimed to identify the TME population instructed by the tumor's immunosuppression signals guided by ionizing radiation. A SurvivalGenie[25]-based TCGA-GBM survival analysis, leveraging gene sets reflective of TME subsets, unveiled a significant survival advantage associated with a lower expression of the macrophage gene signature (Figure 2A). A re-analysis of available single-cell RNA sequencing datasets[21,28] demonstrated a predominant PD-L1 expression within the macrophage/monocyte/microglia (mac/mono/MG) compartment of glioma murine models, which was mimicked in samples obtained from GBM patients (Figure 2B). Compared to newly diagnosed GBM, recurrent GBM increased the number of CD206-expressing cells at the tumor site (Figure 2B). This receptor exhibits a strong affinity for high mannose oligosaccharides,[29] a type of glycan abundantly present on the surface of EVs.[30] Interestingly, the highest expression of CD206 was observed in the mac/mono/MG compartment, previously described as an endocytic receptor and M2 (macrophages endowed with tumor-promoting capabilities) marker.[31] Other M2 markers (e.g., CD163 & CD204) did not show differential expression when comparing primary and recurrent GBM samples (Figure S2). Prior studies indicate that myeloid cells in the GBM TME have the ability to take up tumor-derived EVs.[12,14] To confirm these observations in the context of radiation *in vivo*, we utilized a modified syngeneic mouse glioma model expressing CT-2A.palm.tdTomato cells. Expression of a palmitoylated form of tdTomato (pTom) in CT-2A cells[32,33] facilitates tracking of tumor-derived membrane fragments, including EVs, within the tumor microenvironment (Figure 2C, top). We implanted these cells into the brains of adult mice, and two weeks later, mice heads received ionizing radiation (2 Gy) for five consecutive days, informed by the observations in Figure 1D and mirroring standard human treatment regimens.[26,27] After twenty days of tumor cell implantation, mice were euthanized, and single-cell suspensions of the tumor area were prepared for flow cytometry analysis (Figure 2C, bottom). In our setup, CD11b-positive ($CD11b^{POS}$) or myeloid cells displayed a 4-fold increased uptake of EVs compared to other immune cells (Figure 2D), regardless of radiation. Our findings suggest a propensity of myeloid cells to take up tumor-derived signals through EVs.

Radiation-induced immune suppression at the GBM site is mitigated by tumor-derived EVs and myeloid recipients

Macrophages are specialized in phagocytosing dead cells or cellular debris.[34] To distinguish the effect resulting from the uptake of EVs by macrophages and conventional phagocytosis in the context of radiation, we intracranially implanted CT-2A.palm.tdTomato.H2B.mCerulean[32,35] cells into mouse brains (Figure 3A). Again, the expression of pTom in CT-2A cells allows tracking of tumor-derived EVs. Additionally, fusion of the nuclear-localized mCerulean (mCer) with H2B histone allows the distinction of EV uptake from whole-cell phagocytosis.[14] Two weeks post-tumor implantation, mice received ionizing radiation (2 Gy) to their head for five consecutive days. Two days after the last irradiation, mice were euthanized, and single-cell suspensions of the tumor area were prepared for flow cytometry analysis (Figure 3B). After gating for cancer cells ($CD45^{NEG}mCer^{POS}pTom^{POS}$), we observed an increase in membrane PD-L1 expression following RT, confirming the results shown in Figure 1D and validating our model (Figure 3C).

Our fluorescent labeling methodology enabled us to discriminate between different types of macrophages based on their interactions: (1) those that did not take up tumor-derived EVs or tumor cells, (2 and 3) those that phagocytosed tumor cells, and (4) those that took up tumor-derived EVs (numbers represent cartoons visualized in Figure 3D). We observed that the bulk (62%) of macrophages ($CD45^{POS}$ $CD11b^{POS}$

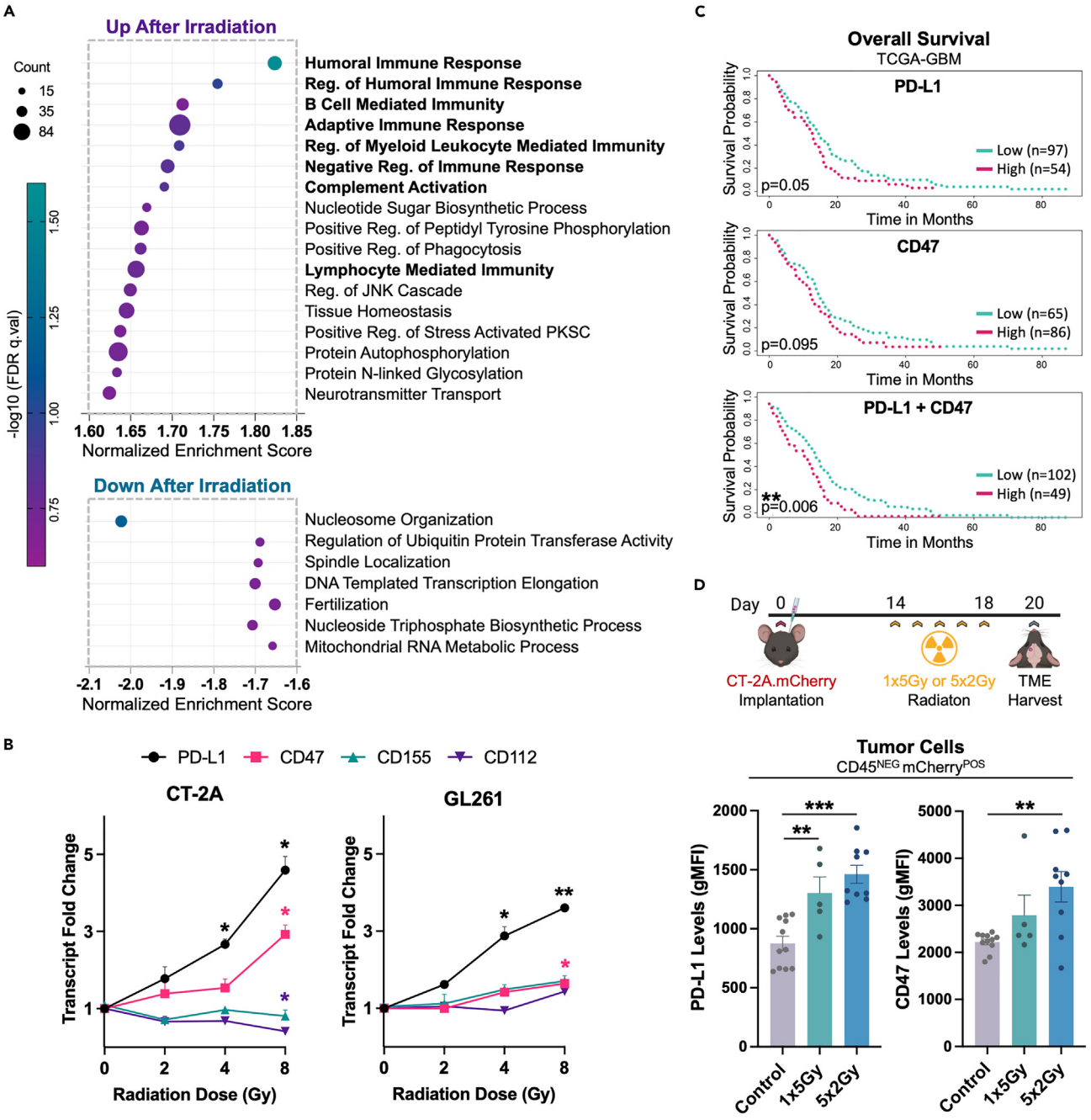

Figure 1. Ionizing radiation induces expression of immune suppressive markers on GBM cells

(A) CT-2A cells were treated with and without 5 Gy ionizing radiation (IR) and assessed by proteomics followed by GSEA pathway analysis.

(B) CT-2A and GL261 cells were exposed to different doses (0, 2, 4, and 8 Gy) of IR and analyzed by qRT-PCR for expression of PD-L1, CD47, CD155, and CD112 (n = 3).

(C) Kaplan-Meier survival curves based on TCGA-GBM dataset computed with individual genes (PD-L1 or CD47) or a combined gene set (PD-L1+CD47).

(D) Tumor-bearing mice were treated with either 1 × 5 Gy or 5 × 2 Gy fractionated ionizing radiation, and PD-L1 and CD47 surface protein expression on $mCherry^{POS}CD45^{NEG}$ (=CT-2A tumor) cells was analyzed by flow cytometry (n ≥ 5). Significance indicated as: *, p < 0.05; **, p < 0.01; ***, p < 0.001; one-way ANOVA or two-tailed, unpaired t test. Data presented as mean ± SEM. See also Figure S1.

$F4/80^{POS}$) in the TME was not directly affected by the tumor (i.e., negative for both mCer and pTom), followed by macrophages that phagocytosed tumor cells (i.e., early phagocytosis is positive for both mCer and pTom (7%) while late phagocytosis (5%) is only positive for mCer), and macrophages that exhibited uptake of tumor-derived EVs (i.e., negative for mCer and positive for pTom [26%]; Figure 3E). To define the

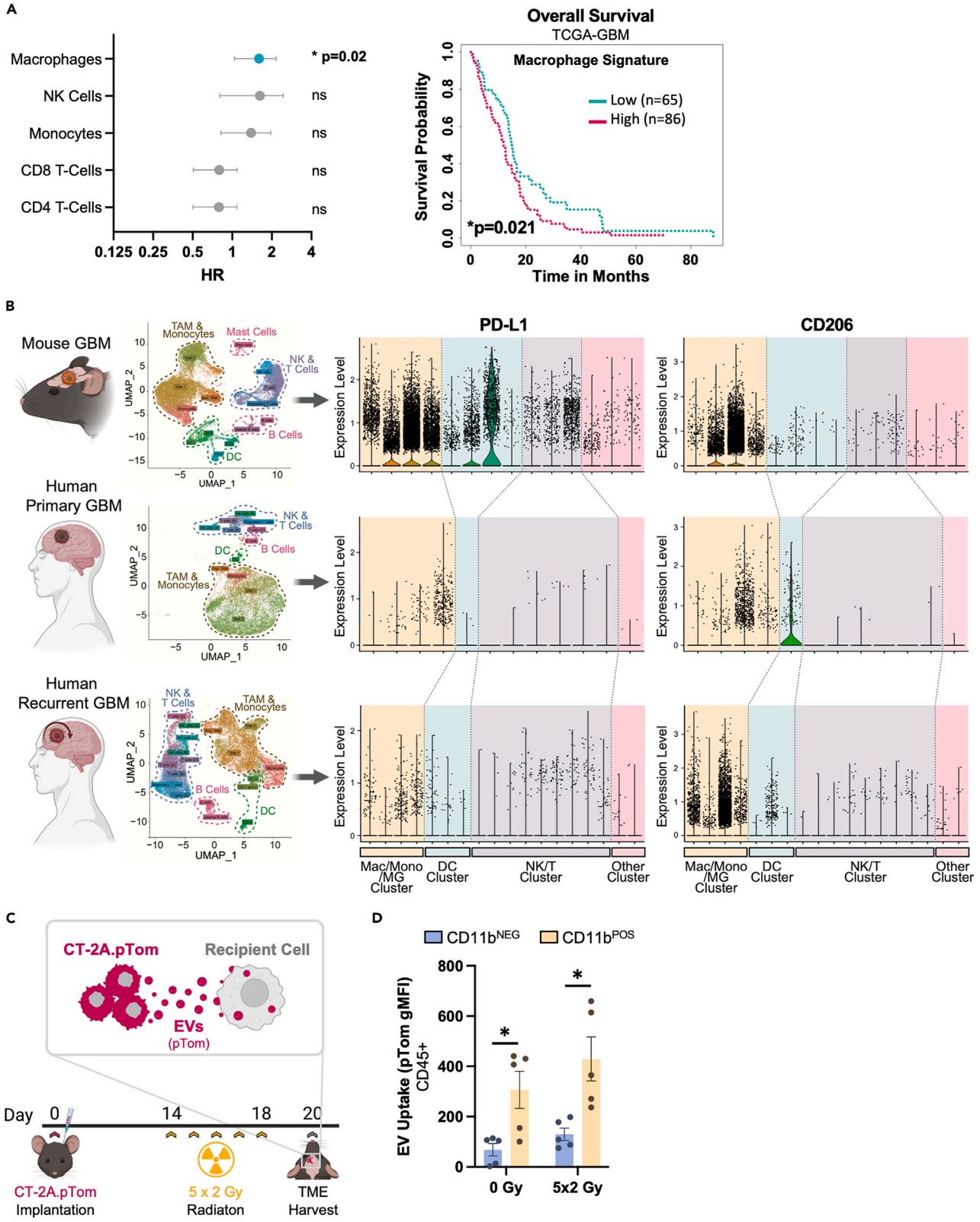
A
Macrophages
NK Cells
Monocytes
CD8 T-Cells
CD4 T-Cells
* p=0.02
ns
ns
ns
ns
0.125 0.25 0.5 1 2 4
HR
Overall Survival
TCGA-GBM
Macrophage Signature
Low (n=65)
High (n=86)
Survival Probability
*p=0.021
Time in Months
B
Mouse GBM
Human Primary GBM
Human Recurrent GBM
TAM & Monocytes
Mast Cells
NK & T Cells
B Cells
DC
UMAP_1
UMAP_2
PD-L1
CD206
Expression Level
Mac/Mono /MG Cluster
DC Cluster
NK/T Cluster
Other Cluster
C
CT-2A.pTom
Recipient Cell
EVs
(pTom)
Day 0
14
18
20
CT-2A.pTom Implantation
5 x 2 Gy Radiaton
TME Harvest
D
CD11b^NEG
CD11b^POS
EV Uptake (pTom gMFI) CD45+
0 Gy
5x2 Gy

Figure 2. The propensity of myeloid cells to take up tumor-derived signals through EVs

(A) Left: Forest plot depicting univariate Cox regression survival analysis of various tumor microenvironment (TME) gene sets in TCGA-GBM dataset, showing the hazard ratio (HR) and 95% confidence intervals. Significant associations are shown in the green-filled HR value circle. A, Right: Kaplan-Meier survival curves based on TCGA-GBM dataset computed with the macrophage gene signature set.

(B) Single-cell RNA sequencing-based analysis of PD-L1 and CD206 expression levels in samples derived from a glioma murine model, human primary GBM, and human recurrent GBM (brainimmuneatlas.org).

(C) Schematic of the *in vivo* strategy to track EV uptake and detailed radiation regimen. C57BL/6 mice were intracranially inoculated with CT-2A.palmtdTomato (CT-2A.pTom) cells. Fourteen days post-injection, mice received a 2 Gy radiotherapy (RT) dose for five consecutive days. Brains were harvested two days post final radiation.

(D) Flow cytometric analysis evaluating EV uptake (pTom gMFI) in $CD45^{POS}CD11b^{NEG}$ or $CD45^{POS}CD11b^{POS}$ cells in the CT-2A TME (mac/mono/MG = macrophages/monocytes/microglia, DC = dendritic cells, NK = natural killer cells, TAM = tumor-associated macrophages/microglia). Significance indicated as: *, $p < 0.05$; two-tailed, unpaired t test. Data presented as mean ± SEM (n = 5). See also Figure S2.

myeloid subpopulation that is most prone to EV uptake, we identified mature macrophages by subgating for $CD45^{POS}$ $CD11b^{POS}$ $F4/80^{POS}$ cells. $F4/80^{POS}$ macrophages contained the highest fraction (23% or 29%) of EV-positive cells, with or without ionizing radiation, respectively (Figure S3A).

To track signature adaptation of immunosuppressive parameters post-uptake of tumor-derived EVs, we monitored PD-L1 levels in myeloid cells. We observed that PD-L1 expression correlated with F4/80 marker expression and that both macrophages that phagocytosed tumor cells and macrophages that took up tumor-derived EVs exhibited increased PD-L1 expression (Figure 3F). The PD-L1 levels in $pTom^{POS}$ macrophages were significantly higher compared to their $mCer^{NEG}$ $pTom^{NEG}$ counterparts, regardless of radiation exposure (Figure 3G).

To analyze whether an increase of PD-L1 in recipient macrophages is due to immune-suppressive adaptation, we tracked CD206, a receptor involved in phagocytosis and mediating EV uptake.[29,30] Interestingly, we observed that CD206 expression in macrophages increased upon radiation, indicating that RT might boost EV uptake in macrophages (Figure 3H). We showed that $CD206^{POS}$ macrophages indeed display an increased pTom signal (Figure 3I). Notably, even though radiation increased the number of $CD206^{POS}$ cells, it did not appear to modulate pTom uptake at the individual cellular level (Figure 3J). Furthermore, we observed that CD206 was a critical marker in distinguishing macrophages that had both $pTom^{POS}$ EVs and PD-L1 (Figure 3K). Interestingly, tumor-derived EV-uptake resulted in higher PD-L1 in $CD206^{POS}$ macrophages than phagocytosis of tumor cells.

To avoid a potential bias in our findings based on phagocytosis of $pTom^{POS}$ $mCer^{NEG}$ tumor cells, we evaluated the expression of the nuclear marker Ki67, which is highly present in tumor cell nuclei due to their high proliferation rate.[36] Ki67 accounts for the potential loss of the mCer transgene due to transgene instability after engrafting tumor cells in the mouse brain (Figure 3L). Radiation did not induce significant changes in Ki67 expression in CT-2A cells (Figure S3B) or macrophages (Figure 3M). As expected, macrophages positive for Ki67 also expressed higher levels of nuclear-bound mCer, independent of radiation (Figure 3N). Ki67 expression was found to be a determining factor for PD-L1 expression solely in $mCer^{POS}$ $pTom^{POS}$ macrophages, as depicted in Figure 3O. These results show that the presence of $pTom^{POS}$ macrophages is likely attributed to the uptake of tumor-derived EVs, rather than arising from phagocytosis of a tumor cell that was $pTom^{POS}$ $mCer^{NEG}$. In summary, our findings indicate that the uptake of tumor-derived EVs by macrophages contributes to increased PD-L1 expression by $CD206^{POS}$ macrophages at the tumor site, which is modulated by RT.

Effect of tumor-derived EVs on macrophage cytokine secretion and phagocytosis

In vivo tracking does not allow for detailed interrogation of the cause and effect of tumor-derived EVs. To dissect the impact of tumor-derived EVs on macrophage activation, we exposed primary bone-marrow-derived macrophages (BMDM) to GBM-EVs isolated by size-exclusion chromatography. RT did not have a significant impact on EV size, secretion, or EV marker protein expression (Figures S4A–S4D). We first confirmed uptake of pTom-labeled EVs by BMDM using fluorescence analysis (Figures 4A and S4E). BMDMs were exposed to ionizing radiation (BMDM+5 Gy), CT-2A-derived EVs (BMDM+EV), and EVs derived from irradiated CT-2A cells (BMDM+irEV) and thoroughly washed to avoid confounding signals caused by donor-EVs (Figure 4B). To probe the immune regulatory effect of tumor-derived EVs on macrophages, we conducted proteomic analyses on BMDM exposed to CT-2A-derived EVs with and without irradiation. GSEA analysis focusing on immune-related pathways revealed that exposure to CT-2A EVs (BMDM+EV) and to EVs derived from irradiated CT-2A cells (BMDM+irEV) led to the upregulation of immune-related signaling in macrophages (Figure 4C). No immune-related pathways were detected in the top 20 significantly downregulated pathways in EV-treated BMDM. Furthermore, BMDM exposed to tumor-derived EVs displayed an increased secretion of chemokines and MMPs, suggesting that EVs can provide cues to induce a pro-tumorigenic macrophage response (Figures 4D, S4F, and S4G). Notably, EVs derived from irradiated CT-2A cells led to an increase in cytokines known to mediate radioresistance, such as CXCL1.[37]

As the increased release of cytokines by macrophages indicates enhanced tumor immunity participation (Figure 4D), we explored this further and focused on macrophage phagocytosis in response to tumor-derived EV uptake, an essential process for tumor antigen presentation and thus for modulating adaptive tumor immunity.[11] BMDMs were exposed to tumor-derived EVs for 48 h and then co-cultured with pHrodo Red-labeled cancer cells (Figure 4E). As expected, the addition of anti-CD47 antibodies (αCD47) to the co-culture media contributed to increased phagocytosis.[10] Notably, pre-treatment of macrophages with EVs derived from CT-2A cells, treated with and without radiation, enhanced their ability to phagocytose CT-2A cells, regardless of the presence of αCD47 (Figure 4E, Top). Similar effects were also observed with another GBM cell line (005) (Figure 4E, Bottom). We also explored PD-L1 levels on macrophages after tumor-derived EV uptake, a requirement for imposing immune-suppressive ligands to T cells that recognize antigen-MHC complexes post-phagocytosis and

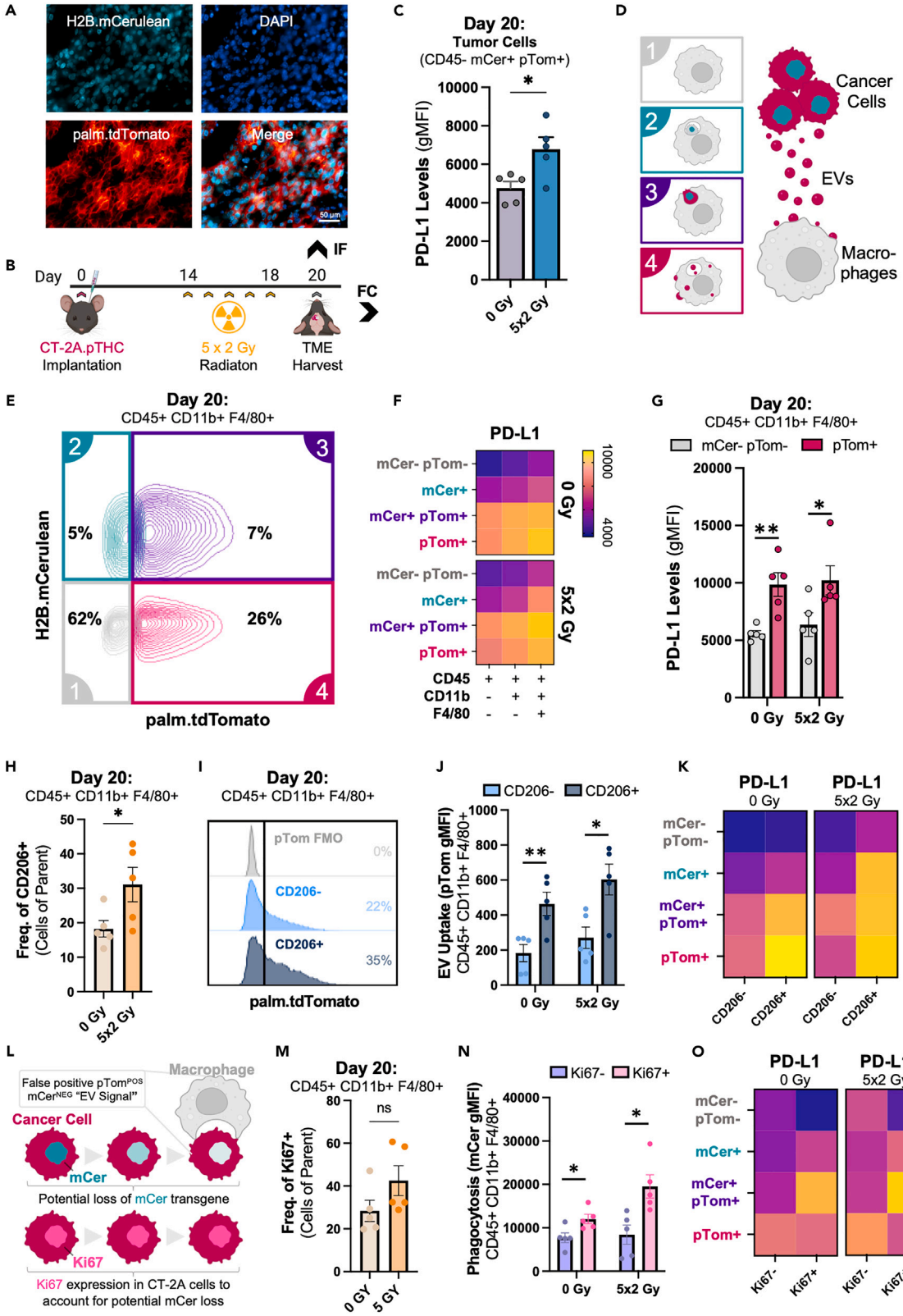
A
H2B.mCerulean
DAPI
palm.tdTomato
Merge
50 µm
B
IF
Day 0 14 18 20
FC
CT-2A.pTHC Implantation
5 x 2 Gy Radiaton
TME Harvest
C
Day 20:
Tumor Cells
(CD45- mCer+ pTom+)
PD-L1 Levels (gMFI)
0 Gy
5x2 Gy
D
Cancer Cells
EVs
Macro-phages
E
Day 20:
CD45+ CD11b+ F4/80+
H2B.mCerulean
palm.tdTomato
5%
7%
62%
26%
F
PD-L1
mCer- pTom-
mCer+
mCer+ pTom+
pTom+
0 Gy
5x2 Gy
CD45 + + +
CD11b - + +
F4/80 - - +
G
Day 20:
CD45+ CD11b+ F4/80+
mCer- pTom-
pTom+
PD-L1 Levels (gMFI)
H
Day 20:
CD45+ CD11b+ F4/80+
Freq. of CD206+ (Cells of Parent)
I
Day 20:
CD45+ CD11b+ F4/80+
pTom FMO
CD206-
22%
CD206+
35%
palm.tdTomato
J
CD206-
CD206+
EV Uptake (pTom gMFI) CD45+ CD11b+ F4/80+
K
PD-L1
0 Gy
PD-L1
5x2 Gy
mCer- pTom-
mCer+
mCer+ pTom+
pTom+
CD206-
CD206+
L
False positive pTomPOS mCerNEG "EV Signal"
Macrophage
Cancer Cell
mCer
Potential loss of mCer transgene
Ki67
Ki67 expression in CT-2A cells to account for potential mCer loss
M
Day 20:
CD45+ CD11b+ F4/80+
ns
Freq. of Ki67+ (Cells of Parent)
0 GY
5 GY
N
Ki67-
Ki67+
Phagocytosis (mCer gMFI) CD45+ CD11b+ F4/80+
O
PD-L1
0 Gy
PD-L1
5x2 Gy
mCer- pTom-
mCer+
mCer+ pTom+
pTom+
Ki67-
Ki67+

Figure 3. Radiation-induced GBM immune suppression is mitigated by tumor-derived EVs and myeloid recipients

C57BL/6 mice were intracranially inoculated with CT-2A.palm.tdTomato.H2B.mCerulean (pTHC) cells. Fourteen days post-implantation, mice brains were irradiated with 2 Gy over 5 days, and 2 days after the last irradiation, tumors were removed for analysis by flow cytometry.

(A) Brain slices analyzed by fluorescence microscopy confirming H2B.mCerulean and palm.tdTomato expression in tumor cells.

(B) Schematic of the *in vivo* strategy to track EV uptake and detailed radiation regimen.

(C) PD-L1 levels (gMFI) in tumor cells ($CD45^{NEG}$ $mCer^{POS}$ $pTom^{POS}$) without (0 Gy) and with (5 × 2Gy) radiation therapy (RT).

(D) Schematic of the strategy to distinguish tumor-derived EV uptake and phagocytosis of tumor cells by macrophages.

(E) Distribution of macrophages in the TME (1) not directly affected by the tumor, (2&3) those that phagocytosed tumor cells, and (4) macrophages that took up tumor-derived EVs.

(F) PD-L1 levels (gMFI) after EV uptake or phagocytosis across myeloid subpopulations.

(G) PD-L1 levels in macrophages that did ($pTom^{POS}$ $mCer^{NEG}$) or did not ($mCer^{NEG}$ $pTom^{NEG}$) take up tumor-derived EVs.

(H) Percentage of $CD206^{POS}$ macrophages in the TME with and without RT.

(I and J) EV uptake (pTom gMFI) analysis in $CD206^{POS}$ and $CD206^{NEG}$ macrophages.

(K) PD-L1 levels (gMFI) after EV uptake or phagocytosis across $CD206^{POS}$ and $CD206^{NEG}$ macrophages with and without RT.

(L) Schematic depicting the strategy to account for potential mCer loss.

(M) Percentage of $Ki67^{POS}$ macrophages with and without RT.

(N) Phagocytosis (mCer gMFI) analysis in $Ki67^{POS}$ and $Ki67^{NEG}$ macrophages.

(O) PD-L1 levels (gMFI) after EV uptake or phagocytosis across $Ki67^{POS}$ and $Ki67^{NEG}$ macrophages with and without RT. Significance indicated as: *, $p < 0.05$; **, $p < 0.01$; one-way ANOVA or two-tailed, unpaired t test. ($n \geq 5$), Data presented as mean ± SEM. mCer = mCerulean, pTom = palm.tdTomato, CT-2A.pTHC = CT-2A.palm.tdTomato.H2B.mCerulean. See also Figure S3.

post-antigen processing. Both CT-2A and 005-derived EVs significantly increased PD-L1 levels in recipient macrophages, with EVs derived from non-irradiated GBM cells exhibiting the highest effect (Figure 4F).

In summary, glioma-derived EVs modulate macrophages by altering their cytokine secretion profile, enhancing phagocytic ability, and increasing PD-L1 expression, which is further modulated by RT.

DISCUSSION

In this study, we aimed to investigate the impact of ionizing radiation on GBM cells and their interactions with the TME. Our findings revealed significant alterations in immune-suppressive markers on GBM cells following exposure to ionizing radiation, including PD-L1 and CD47 immune checkpoint markers. Interestingly, high levels of both PD-L1 and CD47 were associated with poor survival, emphasizing the importance of immune checkpoint regulation in GBM pathogenesis. Importantly, exposure of macrophages to GBM-derived EVs led to an increase in PD-L1 expression. Furthermore, our investigation into the myeloid compartment of the TME highlights the increased presence of CD206-positive macrophages at the tumor site following RT. The uptake of EVs by macrophages was associated with high PD-L1 expression, indicating their potential to induce a pro-oncogenic environment in the TME, facilitating tumor progression and therapeutic resistance.

Our observations regarding dose-dependent response of PD-L1 and CD47 to radiation in glioma models are consistent with previous studies in various cancer types.[38–40] Notably, expression of CD47 appears to be influenced by radiation in a context-dependent manner, either increasing[41–43] or decreasing,[44] depending on the cell/tissue type and radiation regimen. Increased CD206-expressing myeloid cells in more aggressive recurrent GBM samples compared to newly diagnosed cases supports previous findings, indicating the role of myeloid cells in GBM tumor immune escape.[45] Our observations also align with prior studies that have demonstrated the active modulation of the TME through GBM-secreted EVs.[14,46] We identified a potential propensity of high CD206-expressing macrophages to take up EVs, suggesting the enrichment of high mannose glycans on the EV surface, making them an ideal tool for delivery of therapeutics into CD206-expressing TAMs.[29,30]

Previous studies have highlighted the effects of tumor-derived EVs on macrophages/monocytes.[12,13,15,16] In our study, we aimed to integrate past findings into a more holistic *in vivo* model and further investigated the impact of RT as an additional dimension to the complex interplay between GBM, EVs, RT, and myeloid cells in the TME. Dissecting the cause and effect of EV-mediated TME modulation *in vivo* without introducing confounding variables poses significant challenges. Given that PD-L1 expression on macrophages plays a crucial role in immune suppression within the TME, and to corroborate our *in vivo* results, we examined the expression of PD-L1 on BMDM in culture following EV treatment. EVs derived from GBM cells increased PD-L1 expression on macrophages. Given that ionizing radiation leads to an increase in PD-L1 in GBM cells, we expected a more increased expression of PD-L1 on irEV-treated macrophages. However, this effect was relatively lower compared to the GBM control EV condition, hinting toward a more indirect mechanism (instead of direct PD-L1 protein transfer) underlying EV-induced upregulation of PD-L1. Previous studies demonstrated that glioma cell phagocytosis by BMDMs in the TME leads to the formation of TAMs with increased immunosuppressive phenotypes by expressing immune-checkpoint proteins like PD-L1.[11] Our data indicate that EVs are taken up by macrophages, leading to an increase in phagocytosis of PD-L1-rich GBM cells and, consequently, to a higher PD-L1 expression on macrophages. Interestingly, the enhanced phagocytic capacity of BMDM following exposure to GBM EVs continued even upon blocking with anti-CD47, implying the presence of additional mechanisms involved beyond the CD47-SIRPa signaling pathway.[18]

In conclusion, our study sheds light on the immunomodulatory effects of ionizing radiation in GBM and their interactions with the TME. The immunosuppressive environment in response to radiation therapy, including checkpoint markers such as PD-L1, is partly adopted by tumor-secreted EVs. These EVs can impose an "immune-suppressive halo" around tumor cells in a non-RT-dependent manner through modulation of specific macrophage subsets in the TME by providing bait (i.e., antigen by enhanced phagocytosis) for T cells while blocking the latter with high levels of PD-L1. Continuing research in this area is crucial to identify targets that can overcome immunotherapy failures for GBM.

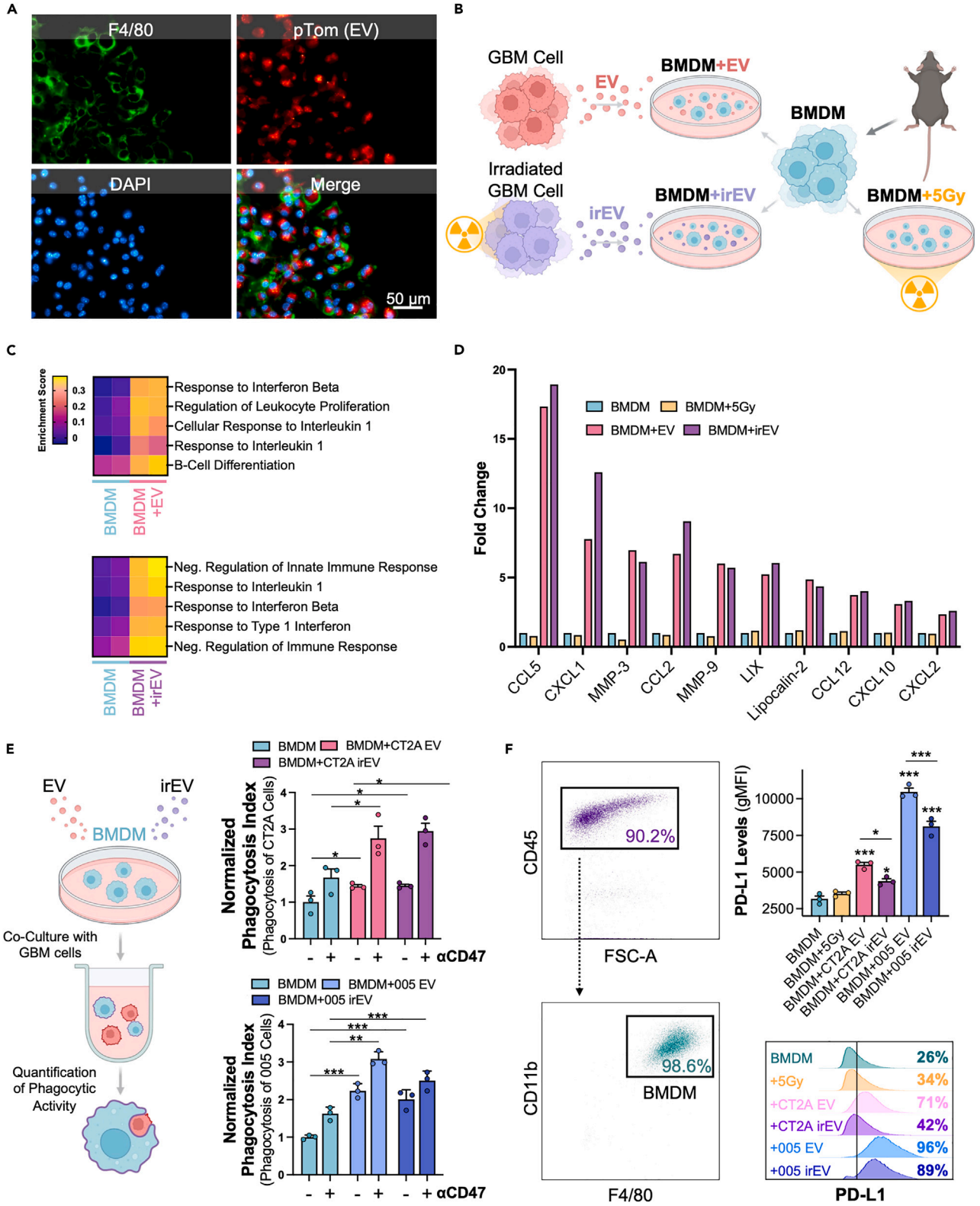

Figure 4. Effect of tumor-derived EVs on bone-marrow-derived macrophage cytokine secretion, phagocytosis, and PD-L1 expression

(A) Bone-marrow-derived macrophages (BMDMs) were exposed to palm.tdTomato (pTom)-labeled EVs, fixed and stained for F4/80 (macrophage marker; green) and DAPI (blue), and EV uptake was analyzed by fluorescence analysis.

Figure 4. *Continued*

(B–D) BMDM were exposed to EVs derived from untreated (BMDM+EV) or irradiated (BMDM+irEV) CT-2A cells. Schematic of experimental setup (B). GSEA pathway analysis showing significantly upregulated immune-related pathways (n = 2) in CT-2A EV and irEV-treated BMDM (C). Graph bar showing cytokine array results of BMDM exposed to 5 Gy radiation (BMDM+5 Gy), EV, or irEV depicting the top 10 differentially expressed cytokines (D).

(E) BMDM exposed to EVs or irEVs were co-cultured with CT2A or 005 glioma cells labeled with pHrodo Red, pre-treated with and without anti-CD47, and analyzed for phagocytic ability by flow cytometry. Experimental setup schematic (Left). Graph depicting the phagocytosis index of BMDM under different conditions (Right).

(F) BMDM exposed to 5 Gy RT or EVs/irEVs from CT-2A or 005 glioma cells were analyzed for PD-L1 levels. Gating strategy to identify BMDM ($CD45^{POS}$ $CD11b^{POS}$ $F4/80^{POS}$) (Left). Analysis of PD-L1 levels (gMFI) in BMDM under different conditions by flow cytometry (Right). Significance indicated as: *, $p < 0.05$; **, $p < 0.01$; ***, $p < 0.001$; one-way ANOVA. ($n \geq 3$), Data presented as mean ± SEM. See also Figure S4.

Limitations of the study

In vivo tracking of EV uptake provided valuable insights into the complex interaction between ionizing radiation, immune-suppressive markers, and tumor-derived EVs in GBM. We used a palmitoylated form of tdTomato to capture a wide range of tumor-derived EVs, which may introduce a portion of non-EV particles and fragments. Our main goal was to provide a holistic overview of the effect of all tumor-secreted EV subtypes (including exosomes, microvesicles, and apoptotic bodies) as reflected in an actual tumor setting. Future studies may use more targeted labeling to investigate which EV subpopulation is the main driver of the observed effect. A more in-depth investigation is required to elucidate the precise mechanisms underlying EV uptake and the specific immunomodulatory effect on myeloid cells. Based on our findings, future research directions may focus on exploring underlying mechanisms of immune checkpoint marker upregulation in response to ionizing radiation. Past studies have highlighted the role of EGFR autophosphorylation following RT[47] and its potential involvement in subsequent PD-L1 upregulation in glioma cells.[39] Future studies are needed to pinpoint the exact mechanisms involved, especially when it comes to CD47. We chose well-established radiation protocols that closely mimic human RT regimens or have been used to boost immunotherapy.[26,27] Future approaches may investigate the effect of alternative radiation regimens on TME interactions, which could provide further insights into the potential optimization of radiation therapy for GBM. Moreover, future studies are necessary to elucidate the underlying mechanisms by which EVs modulate macrophages, particularly focusing on EV secretion, uptake dynamics, and EV content. Detailed identification of the specific cargo within EVs responsible for inducing the immune-suppressive phenotype in macrophages would be of great significance. Understanding these mechanisms could pave the way for developing strategies to reverse the immune-suppressive effects of tumor-derived EVs and potentially enhance the efficacy of immunotherapies and RT in GBM.

STAR★METHODS

Detailed methods are provided in the online version of this paper and include the following:

- KEY RESOURCES TABLE
- RESOURCE AVAILABILITY
  - Lead contact
  - Materials availability
  - Data and code availability
- EXPERIMENTAL MODEL AND STUDY PARTICIPANT DETAILS
  - Animals
  - Cultured cells
- METHOD DETAILS
  - Radiation therapy
  - Quantitative proteomics
  - RNA isolation and quantitative real-time PCR (q-PCR)
  - TCGA-GBM survival analyses
  - Cell transduction
  - Intracranial tumor injections
  - Flow cytometry
  - Single cell RNA-sequencing dataset analysis
  - Immunohistochemistry
  - Bone marrow-derived macrophage isolation
  - EV isolation
  - EV quantification
  - Western blot
  - EV treatment
  - Cytokine array
  - Phagocytosis assay
- QUANTIFICATION AND STATISTICAL ANALYSIS

SUPPLEMENTAL INFORMATION

Supplemental information can be found online at https://doi.org/10.1016/j.isci.2024.108807.

ACKNOWLEDGMENTS

This work was supported by grants from the National Institutes of Health, the National Cancer Institute P01CA069246 (BAT), and NIH NINDS R01 5R01NS122163 (BAT and KB). Parts of some figures were created with BioRender.com. The authors would like to thank Lisa Nieland and Erik Abels for their valuable input, Tianhe Xiao for producing the viral vectors in the MGH vector core (supported by NIH/NINDS P30NS04776), and the Mass General Cancer Center Translational Cartography Core, which provided support for confocal imaging.

AUTHOR CONTRIBUTIONS

M.W.S.: conceptualization, data curation, investigation, software, formal analysis, validation, visualization, methodology, writing – original draft, and writing – review and editing. Z.A.: software, data curation, investigation, formal analysis, and methodology. P.R.: data curation, investigation, software, formal analysis, and writing – original draft. R.M.: software, data curation, investigation, formal analysis, and methodology. S.M.: investigation. M.H.: investigation. E.Z.: investigation. D.P.N.: supervision, writing – original draft, writing – review and editing, conceptualization, and validation. W.H.: software, supervision, and methodology. K.B.: data curation, resources, supervision, validation, software, formal analysis, writing – original draft, and writing – review and editing. B.A.T.: conceptualization, resources, supervision, funding acquisition, validation, project administration, and writing – review and editing.

DECLARATION OF INTERESTS

The authors declare no competing interests.

Received: September 6, 2023
Revised: November 10, 2023
Accepted: January 2, 2024
Published: January 5, 2024

REFERENCES

1. Ostrom, Q.T., Price, M., Neff, C., Cioffi, G., Waite, K.A., Kruchko, C., and Barnholtz-Sloan, J.S. (2022). CBTRUS Statistical Report: Primary Brain and Other Central Nervous System Tumors Diagnosed in the United States in 2015–2019. Neuro Oncol. *24*, v1–v95.
2. Bao, S., Wu, Q., McLendon, R.E., Hao, Y., Shi, Q., Hjelmeland, A.B., Dewhirst, M.W., Bigner, D.D., and Rich, J.N. (2006). Glioma stem cells promote radioresistance by preferential activation of the DNA damage response. Nature *444*, 756–760.
3. Osuka, S., and Van Meir, E.G. (2017). Overcoming therapeutic resistance in glioblastoma: the way forward. J. Clin. Invest. *127*, 415–426.
4. Keime-Guibert, F., Chinot, O., Taillandier, L., Cartalat-Carel, S., Frenay, M., Kantor, G., Guillamo, J.-S., Jadaud, E., Colin, P., Bondiau, P.-Y., et al. (2007). Radiotherapy for Glioblastoma in the Elderly. N. Engl. J. Med. *356*, 1527–1535.
5. Hardee, M.E., Marciscano, A.E., Medina-Ramirez, C.M., Zagzag, D., Narayana, A., Lonning, S.M., and Barcellos-Hoff, M.H. (2012). Resistance of Glioblastoma-Initiating Cells to Radiation Mediated by the Tumor Microenvironment Can Be Abolished by Inhibiting Transforming Growth Factor-β. Cancer Res. *72*, 4119–4129.
6. Bhat, K.P.L., Balasubramaniyan, V., Vaillant, B., Ezhilarasan, R., Hummelink, K., Hollingsworth, F., Wani, K., Heathcock, L., James, J.D., Goodman, L.D., et al. (2013). Mesenchymal Differentiation Mediated by NF-κB Promotes Radiation Resistance in Glioblastoma. Cancer Cell *24*, 331–346.
7. Shu, H.K., Kim, M.M., Chen, P., Furman, F., Julin, C.M., and Israel, M.A. (1998). The intrinsic radioresistance of glioblastoma-derived cell lines is associated with a failure of p53 to induce p21BAX expression. Proc. Natl. Acad. Sci. USA *95*, 14453–14458.
8. Quail, D.F., and Joyce, J.A. (2017). The Microenvironmental Landscape of Brain Tumors. Cancer Cell *31*, 326–341.
9. Buonfiglioli, A., and Hambardzumyan, D. (2021). Macrophages and microglia: the cerberus of glioblastoma. Acta Neuropathol. Commun. *9*, 54.
10. von Roemeling, C.A., Wang, Y., Qie, Y., Yuan, H., Zhao, H., Liu, X., Yang, Z., Yang, M., Deng, W., Bruno, K.A., et al. (2020). Therapeutic modulation of phagocytosis in glioblastoma can activate both innate and adaptive antitumour immunity. Nat. Commun. *11*, 1508.
11. Wu, M., Wu, L., Wu, W., Zhu, M., Li, J., Wang, Z., Li, J., Ding, R., Liang, Y., Li, L., et al. (2023). Phagocytosis of glioma cells enhances the immunosuppressive phenotype of bone marrow-derived macrophages. Cancer Res. *83*, 771–785.
12. de Vrij, J., Maas, S.L.N., Kwappenberg, K.M.C., Schnoor, R., Kleijn, A., Dekker, L., Luider, T.M., de Witte, L.D., Litjens, M., van Strien, M.E., et al. (2015). Glioblastoma-derived extracellular vesicles modify the phenotype of monocytic cells. Int. J. Cancer *137*, 1630–1642.
13. Jung, M.-Y., Aibaidula, A., Brown, D.A., Himes, B.T., Cumba Garcia, L.M., and Parney, I.F. (2022). Superinduction of immunosuppressive glioblastoma extracellular vesicles by IFN-γ through PD-L1 and IDO1. Neurooncol. Adv. *4*, vdac017.
14. Abels, E.R., Maas, S.L.N., Nieland, L., Wei, Z., Cheah, P.S., Tai, E., Kolsteeg, C.-J., Dusoswa, S.A., Ting, D.T., Hickman, S., et al. (2019). Glioblastoma-Associated Microglia Reprogramming Is Mediated by Functional Transfer of Extracellular miR-21. Cell Rep. *28*, 3105–3119.e7.
15. Himes, B.T., Peterson, T.E., de Mooij, T., Parney, D., Garcia, L.M.C., Jung, M.-Y., Uhm, S., Yan, D., Tyson, J., et al. (2020). The role of extracellular vesicles and PD-L1 in glioblastoma-mediated immunosuppressive monocyte induction. Neuro Oncol. *22*, 967–978.
16. Gabrusiewicz, K., Li, X., Wei, J., Hashimoto, Y., Marisetty, A.L., Ott, M., Wang, F., Hawke, D., Yu, J., Healy, L.M., et al. (2018). Glioblastoma stem cell-derived exosomes induce M2 macrophages and PD-L1 expression on human monocytes. OncoImmunology *7*, e1412909.
17. Iwai, Y., Ishida, M., Tanaka, Y., Okazaki, T., Honjo, T., and Minato, N. (2002). Involvement of PD-L1 on tumor cells in the escape from host immune system and tumor immunotherapy by PD-L1 blockade. Proc. Natl. Acad. Sci. *99*, 12293–12297.
18. Willingham, S.B., Volkmer, J.-P., Gentles, A.J., Sahoo, D., Dalerba, P., Mitra, S.S., Wang, J., Contreras-Trujillo, H., Martin, R., Cohen, J.D., et al. (2012). The CD47-signal regulatory protein alpha (SIRPa) interaction is a therapeutic target for human solid tumors. Proc. Natl. Acad. Sci. *109*, 6662–6667.
19. Binello, E., Qadeer, Z.A., Kothari, H.P., Emdad, L., and Germano, I.M. (2012). Stemness of the CT-2A Immunocompetent Mouse Brain Tumor Model: Characterization In Vitro. J. Cancer *3*, 166–174.
20. Khalsa, J.K., Cheng, N., Keegan, J., Chaudry, A., Driver, J., Bi, W.L., Lederer, J., and Shah, K. (2020). Immune phenotyping of diverse syngeneic murine brain tumors identifies

immunologically distinct types. Nat. Commun. *11*, 3912.
21. Pombo Antunes, A.R., Scheyltjens, I., Lodi, F., Messiaen, J., Antoranz, A., Duerinck, J., Kancheva, D., Martens, L., De Vlaminck, K., Van Hove, H., et al. (2021). Single-cell profiling of myeloid cells in glioblastoma across species and disease stage reveals macrophage competition and specialization. Nat. Neurosci. *24*, 595–610.
22. Zeng, T., Cao, Y., Jin, T., Tian, Y., Dai, C., and Xu, F. (2021). The CD112R/CD112 axis: a breakthrough in cancer immunotherapy. J. Exp. Clin. Cancer Res. *40*, 285.
23. Sloan, K.E., Stewart, J.K., Treloar, A.F., Matthews, R.T., and Jay, D.G. (2005). CD155/PVR Enhances Glioma Cell Dispersal by Regulating Adhesion Signaling and Focal Adhesion Dynamics. Cancer Res. *65*, 10930–10937.
24. Cancer Genome Atlas Research Network, Weinstein, J.N., Collisson, E.A., Mills, G.B., Shaw, K.R.M., Ozenberger, B.A., Ellrott, K., Shmulevich, I., Sander, C., Stuart, J.M., et al. (2013). The Cancer Genome Atlas Pan-Cancer analysis project. Nat. Genet. *45*, 1113–1120.
25. Dwivedi, B., Mumme, H., Satpathy, S., Bhasin, S.S., and Bhasin, M. (2022). Survival Genie, a web platform for survival analysis across pediatric and adult cancers. Sci. Rep. *12*, 3069.
26. Leder, K., Pitter, K., LaPlant, Q., Hambardzumyan, D., Ross, B.D., Chan, T.A., Holland, E.C., and Michor, F. (2014). Mathematical Modeling of PDGF-Driven Glioblastoma Reveals Optimized Radiation Dosing Schedules. Cell *156*, 603–616.
27. Tian, T., Liang, R., Erel-Akbaba, G., Saad, L., Obeid, P.J., Gao, J., Chiocca, E.A., Weissleder, R., and Tannous, B.A. (2022). Immune Checkpoint Inhibition in GBM Primed with Radiation by Engineered Extracellular Vesicles. ACS Nano *16*, 1940–1953.
28. Van Hove, H., Martens, L., Scheyltjens, I., De Vlaminck, K., Pombo Antunes, A.R., De Prijck, S., Vandamme, N., De Schepper, S., Van Isterdael, G., Scott, C.L., et al. (2019). A single-cell atlas of mouse brain macrophages reveals unique transcriptional identities shaped by ontogeny and tissue environment. Nat. Neurosci. *22*, 1021–1035.
29. Fiani, M.L., Barreca, V., Sargiacomo, M., Ferrantelli, F., Manfredi, F., and Federico, M. (2020). Exploiting Manipulated Small Extracellular Vesicles to Subvert Immunosuppression at the Tumor Microenvironment through Mannose Receptor/CD206 Targeting. Int. J. Mol. Sci. *21*, 6318.
30. Gerlach, J.Q., and Griffin, M.D. (2016). Getting to know the extracellular vesicle glycome. Mol. Biosyst. *12*, 1071–1081.
31. Liu, J., Geng, X., Hou, J., and Wu, G. (2021). New insights into M1/M2 macrophages: key modulators in cancer progression. Cancer Cell Int. *21*, 389.
32. Lai, C.P., Kim, E.Y., Badr, C.E., Weissleder, R., Mempel, T.R., Tannous, B.A., and Breakefield, X.O. (2015). Visualization and tracking of tumour extracellular vesicle delivery and RNA translation using multiplexed reporters. Nat. Commun. *6*, 7029.
33. van der Vos, K.E., Abels, E.R., Zhang, X., Lai, C., Carrizosa, E., Oakley, D., Prabhakar, S., Mardini, O., Crommentuijn, M.H.W., Skog, J., et al. (2016). Directly visualized glioblastoma-derived extracellular vesicles transfer RNA to microglia/macrophages in the brain. Neuro Oncol. *18*, 58–69.
34. Murray, P.J., and Wynn, T.A. (2011). Protective and pathogenic functions of macrophage subsets. Nat. Rev. Immunol. *11*, 723–737.
35. Welm, B.E., Dijkgraaf, G.J.P., Bledau, A.S., Welm, A.L., and Werb, Z. (2008). Lentiviral Transduction of Mammary Stem Cells for Analysis of Gene Function during Development and Cancer. Cell Stem Cell *2*, 90–102.
36. LI, L.T., JIANG, G., CHEN, Q., and ZHENG, J.N. (2015). Ki67 is a promising molecular target in the diagnosis of cancer (Review). Mol. Med. Rep. *11*, 1566–1572.
37. Zhang, H., Yue, J., Jiang, Z., Zhou, R., Xie, R., Xu, Y., and Wu, S. (2017). CAF-secreted CXCL1 conferred radioresistance by regulating DNA damage response in a ROS-dependent manner in esophageal squamous cell carcinoma. Cell Death Dis. *8*, e2790.
38. Zhang, P., Miska, J., Lee-Chang, C., Rashidi, A., Panek, W.K., An, S., Zannikou, M., Lopez-Rosas, A., Han, Y., Xiao, T., et al. (2019). Therapeutic targeting of tumor-associated myeloid cells synergizes with radiation therapy for glioblastoma. Proc National Acad Sci *116*, 23714–23723.
39. Song, X., Shao, Y., Jiang, T., Ding, Y., Xu, B., Zheng, X., Wang, Q., Chen, X., Gu, W., Wu, C., and Jiang, J. (2018). Radiotherapy Upregulates Programmed Death Ligand-1 through the Pathways Downstream of Epidermal Growth Factor Receptor in Glioma. EBioMedicine *28*, 105–113.
40. Deng, L., Liang, H., Burnette, B., Beckett, M., Darga, T., Weichselbaum, R.R., and Fu, Y.-X. (2014). Irradiation and anti–PD-L1 treatment synergistically promote antitumor immunity in mice. J. Clin. Invest. *124*, 687–695.
41. Candas-Green, D., Xie, B., Huang, J., Fan, M., Wang, A., Menaa, C., Zhang, Y., Zhang, L., Jing, D., Azghadi, S., et al. (2020). Dual blockade of CD47 and HER2 eliminates radioresistant breast cancer cells. Nat. Commun. *11*, 4591.
42. Rostami, E., Bakhshandeh, M., Ghaffari-Nazari, H., Alinezhad, M., Alimohammadi, M., Alimohammadi, R., Mahmoodi Chalbatani, G., Hejazi, E., Webster, T.J., Tavakkol-Afshari, J., and Jalali, S.A. (2022). Combining ablative radiotherapy and anti CD47 monoclonal antibody improves infiltration of immune cells in tumor microenvironments. PLoS One *17*, e0273547.
43. Wan, X., Fang, M., Chen, T., Wang, H., Zhou, Q., Wei, Y., Zheng, L., Zhou, Y., and Chen, K. (2022). The mechanism of low-dose radiation-induced upregulation of immune checkpoint molecule expression in lung cancer cells. Biochem. Biophys. Res. Commun. *608*, 102–107.
44. Vermeer, D.W., Spanos, W.C., Vermeer, P.D., Bruns, A.M., Lee, K.M., and Lee, J.H. (2013). Radiation-induced loss of cell surface CD47 enhances immune-mediated clearance of human papillomavirus-positive cancer. Int. J. Cancer *133*, 120–129.
45. Akkari, L., Bowman, R.L., Tessier, J., Klemm, F., Handgraaf, S.M., de Groot, M., Quail, D.F., Tillard, L., Gadiot, J., Huse, J.T., et al. (2020). Dynamic changes in glioma macrophage populations after radiotherapy reveal CSF-1R inhibition as a strategy to overcome resistance. Sci. Transl. Med. *12*, eaaw7843.
46. Ricklefs, F.L., Alayo, Q., Krenzlin, H., Mahmoud, A.B., Speranza, M.C., Nakashima, H., Hayes, J.L., Lee, K., Balaj, L., Passaro, C., et al. (2018). Immune evasion mediated by PD-L1 on glioblastoma-derived extracellular vesicles. Sci. Adv. *4*, eaar2766.
47. Kiyozuka, M., Akimoto, T., Fukutome, M., Motegi, A., and Mitsuhashi, N. (2013). Radiation-induced dimer formation of EGFR: implications for the radiosensitizing effect of cetuximab. Anticancer Res. *33*, 4337–4346.
48. Marumoto, T., Tashiro, A., Friedmann-Morvinski, D., Scadeng, M., Soda, Y., Gage, F.H., and Verma, I.M. (2009). Development of a novel mouse glioma model using lentiviral vectors. Nat. Med. *15*, 110–116.
49. Ting, L., Rad, R., Gygi, S.P., and Haas, W. (2011). MS3 eliminates ratio distortion in isobaric multiplexed quantitative proteomics. Nat. Methods *8*, 937–940.
50. McAlister, G.C., Nusinow, D.P., Jedrychowski, M.P., Wühr, M., Huttlin, E.L., Erickson, B.K., Rad, R., Haas, W., and Gygi, S.P. (2014). MultiNotch MS3 Enables Accurate, Sensitive, and Multiplexed Detection of Differential Expression across Cancer Cell Line Proteomes. Anal. Chem. *86*, 7150–7158.
51. Edwards, A., and Haas, W. (2016). Proteomics in Systems Biology, Methods and Protocols. Methods Mol. Biol. *1394*, 1–13.
52. Lapek, J.D., Greninger, P., Morris, R., Amzallag, A., Pruteanu-Malinici, I., Benes, C.H., and Haas, W. (2017). Detection of dysregulated protein-association networks by high-throughput proteomics predicts cancer vulnerabilities. Nat. Biotechnol. *35*, 983–989.
53. Li, J., Van Vranken, J.G., Pontano Vaites, L., Schweppe, D.K., Huttlin, E.L., Etienne, C., Nandhikonda, P., Viner, R., Robitaille, A.M., Thompson, A.H., et al. (2020). TMTpro reagents: a set of isobaric labeling mass tags enables simultaneous proteome-wide measurements across 16 samples. Nat. Methods *17*, 399–404.
54. Eng, J.K., McCormack, A.L., and Yates, J.R. (1994). An approach to correlate tandem mass spectral data of peptides with amino acid sequences in a protein database. J. Am. Soc. Mass Spectrom. *5*, 976–989.
55. Elias, J.E., and Gygi, S.P. (2007). Target-decoy search strategy for increased confidence in large-scale protein identifications by mass spectrometry. Nat. Methods *4*, 207–214.
56. Huttlin, E.L., Jedrychowski, M.P., Elias, J.E., Goswami, T., Rad, R., Beausoleil, S.A., Villén, J., Haas, W., Sowa, M.E., and Gygi, S.P. (2010). A Tissue-Specific Atlas of Mouse Protein Phosphorylation and Expression. Cell *143*, 1174–1189.
57. Hao, Y., Hao, S., Andersen-Nissen, E., Mauck, W.M., Zheng, S., Butler, A., Lee, M.J., Wilk, A.J., Darby, C., Zager, M., et al. (2021). Integrated analysis of multimodal single-cell data. Cell *184*, 3573–3587.e29.
58. Toda, G., Yamauchi, T., Kadowaki, T., and Ueki, K. (2021). Preparation and culture of bone marrow-derived macrophages from mice for functional analysis. STAR Protoc. *2*, 100246.

STAR★METHODS

KEY RESOURCES TABLE

REAGENT or RESOURCE	SOURCE	IDENTIFIER
Antibodies		
Brilliant Violet 785 anti-mouse/human CD11b	Biolegend	Cat# 101243; RRID: AB_2561373
PerCP-eFluor 710 anti-mouse CD206	Invitrogen	Cat# 46-2061-82; RRID: AB_2784688
Alexa Fluor 488 anti-mouse CD45	Biolegend	Cat# 103121; RRID: AB_493532
Alexa Fluor 700 anti-mouse/human Ki-67	Invitrogen	Cat# 56-5698-82; RRID: AB_2637480
APC anti-mouse CD274 (B7-H1, PD-L1)	Biolegend	Cat# 124311; RRID: AB_10612935
APC/Cyanine7 anti-mouse F4/80	Biolegend	Cat# 123117; RRID: AB_893489
TruStain fcX (anti-mouse Cd16/32)	BioLegend	Cat# 101319; RRID: AB_1574973
Alexa Fluor 488 anti-mouse F4/80	Biolegend	Cat# 123119; RRID: AB_893491
β-actin	Cell Signaling Technology	Cat# 4967
Alix	Santa Cruz Biotechnology	Cat# sc-53538
CD81	Cell Signaling Technology	Cat# 56039S
CD9	Cell Signaling Technology	Cat# 98327S
Anti-rabbit IgG, HRP-linked Antibody	Cell Signaling Technology	Cat# 7074
Anti-mouse IgG, HRP-linked Antibody	Cell Signaling Technology	Cat# 7076
InVivoMAb anti-mouse/human/rat CD47	Bio x Cell	Cat# BE0283; RRID: AB_2687806
Chemicals, peptides, and recombinant proteins		
Dulbecco's Modified Eagle's medium (DMEM)	Corning	Cat# 10-017-CV
Dulbecco's Modified Eagle Medium/Nutrient Mixture F-12 (DMEM/F12)	Gibco	Cat# 11320033
Fetal bovine serum (FBS)	Sigma-Aldrich	Cat# F0926
Penicillin (100 units/ml) and Streptomycin (100 µg/mL) (P/S)	Corning	Cat# 30-002-C
B27 Supplement minus Vitamin A	Gibco	Cat# 12587010
Epidermal growth factor	PeproTech	Cat# AF-100-15
Fibroblast growth factor	PeproTech	Cat# 100-18B
Trypsin-EDTA (0.25%), phenol red	Fisher Scientific	Cat# 25200056
M-CSF recombinant mouse protein	Biolegend	Cat# 576404
Phosphate buffered saline (PBS) 10X	Boston Bioproducts	Cat# BM-220
Xylazine	Santa Cruz	Cat# sc-362950Rx
PFA 32%	Electron Microscopy Sciences	Cat# 15714
VECTASHIELD® Antifade Mounting Medium with DAPI	Vector Labs	Cat# H-1200-10
RBC lysis buffer	eBioscience	Cat# 50-112-9751
RIPA Buffer	Boston-Bioproducts	Cat# BP-115
Halt™ Protease and Phosphatase Inhibitor Cocktail (100X)	Thermo Scientific	Cat# 78440
Pierce™ Bradford Plus Protein Assay Reagent	Thermo Scientific	Cat# 23238
4-12% Bis-Tris NuPage™ gel	Invitrogen	Cat# NP0322BOX
NuPage™ MES SDS Running Buffer	Invitrogen	Cat# NP0002
NuPage™ Transfer Buffer	Invitrogen	Cat# NP00061
SuperSignal™ West Pico Plus Chemiluminescent Substrate	Thermo Scientific	Cat# 34580
CellTrace Violet	Invitrogen	Cat# C34557
pHrodo Red Intracellular pH Indicator Dye	Invitrogen	Cat# P35372

(*Continued on next page*)

Continued

REAGENT or RESOURCE	SOURCE	IDENTIFIER
Live Cell Imaging Solution	Thermo Fisher	Cat# A14291DJ
ZombieUV	Biolegend	Cat# 423107
cOmplete™, EDTA-free Protease Inhibitor Cocktail	Roche	Cat# 04693132001
Bovine Serum Albumin (BSA)	Sigma Aldrich	Cat# A9576-50ML
Dulbecco's Phosphate Buffered Saline (DPBS)	Sigma Aldrich	Cat# D8537-500ML
EDTA	Invitrogen	Cat# 15575020
Tween 20	Sigma Aldrich	Cat# P1379-25ML
Critical commercial assays		
Mycoplasma PCR Detection Kit	abm	Cat# G238
RNeasy mini kit	Qiagen	Cat# 74104
5× All- In-One RT MasterMix kit	abm	Cat# G592
Proteome Profiler Mouse XL Cytokine Array	R&D Systems	Cat# ARY028
eBioscience™ Foxp3/Transcription Factor Staining Buffer Set	Thermo Fisher	Cat# 00-5523-00
TMTpro™ 16plex Label Reagent Set	Thermo Scientific	Cat# A44520
Izon qEVoriginal/70 nm	IZON	Cat# SP1
Deposited data		
scRNA Sequencing Data	Antunes et al.[21]	https://www.brainimmuneatlas.org
UniProtKB	NIF Data Federation	RRID:SCR_004426
Raw proteomics data	MassIVE Repository	MassIVE: MSV000093696
Experimental models: Cell lines		
Mouse: CT-2A	NCI Tumor Repository	CVCL_ZJ44
Mouse: 005	Marumoto et al.[48]	N/A
Mouse: GL261	NCI Tumor Repository	CVCL_Y003
Experimental models: Organisms/strains		
Mouse: C57BL/6	Charles River Laboratory	IMSR_JAX:000664
Oligonucleotides		
mCD274, F: GCTCCAAAGGACTTGTACGTG and R: TGATCTGAAGGGCAGCATTTC	MGH primer bank	https://pga.mgh.harvard.edu/primerbank
mCD47, F: TGGTGGGAAACTACACTTGCG and R: CGTGCGGTTTTTCAGCTCTAT	MGH primer bank	https://pga.mgh.harvard.edu/primerbank
mCD155, F: GGGTGGGGATATACGTGTGC and R: GTTCCTCAGATCCTGTTGGGC	MGH primer bank	https://pga.mgh.harvard.edu/primerbank
mCD112, F: GCATCATTGGAGGTATTATCGCT and R: GAGGGAGGTCCTTCCAGTTC	MGH primer bank	https://pga.mgh.harvard.edu/primerbank
mACTB, F: GGCTGTATTCCCCTCCATCG and R: CCAGTTGGTAACAATGCCATGT	MGH primer bank	https://pga.mgh.harvard.edu/primerbank
mGAPDH, F: AGGTCGGTGTGAACGGATTTG and R: TGTAGACCATGTAGTTGAGGTCA	MGH primer bank	https://pga.mgh.harvard.edu/primerbank
Recombinant DNA		
CSCW2.palmtdTomato	Lai et al.[32]	Breakefield Lab
pHIV-H2B.mCerulean	This paper	Kind gift of Dr. Erik Abels
Software and algorithms		
ImageJ/FIJI	NIH	https://imagej.nih.gov/ij
BioRender	BioRender	https://www.biorender.com

(*Continued on next page*)

Continued

REAGENT or RESOURCE	SOURCE	IDENTIFIER
GraphPad Prism	GraphPad	https://www.graphpad.com
SurvivalGenie	Dwivedi et al.[25]	https://bbisr.shinyapps.winship.emory.edu/SurvivalGenie
R Studio	Open source	https://www.rstudio.com
FlowJo	FlowJo	https://www.flowjo.com
Adobe Illustrator 2023	Adobe	https://www.adpbe.com

RESOURCE AVAILABILITY

Lead contact

Further information and requests for resources and reagents should be directed to and will be fulfilled by the lead contact, Koen Breyne (kbreyne@mgh.harvard.edu).

Materials availability

All unique/stable materials will be made available upon reasonable request from the lead contact without restriction.

Data and code availability

- Proteomics mass spectrometer RAW files can be accessed through the MassIVE data repository (massive.ucsd.edu) under the accession number MSV000093696. All other data reported in this paper will be shared by the lead contact upon request.
- This paper does not report original code.
- Any additional information required to reanalyze the data reported in this paper is available from the lead contact upon request.

EXPERIMENTAL MODEL AND STUDY PARTICIPANT DETAILS

This study does not involve any patients or healthy control participants.

Animals

All animal experiments were approved by the Massachusetts General Hospital Subcommittee on Research Animal Care and complied with guidelines set forth by the National Institutes of Health Guide for the Care and Use of Laboratory Animals. Eight-to-ten weeks old female C57BL/6 (Charles River Lab) mice were used throughout the study. Mice were raised in a temperature and hygrometry-controlled environment on a 12h day/night cycle. Five animals were placed in one cage and animals had access to food and water *ad libitum*.

Cultured cells

CT-2A (RRID:CVCL_ZJ44) (derived from a male mouse brain tumor formed after the intracerebral implantation of 20-methylcholanthrene pellets into C57/BL6 mice[19]) and GL261 (RRID:CVCL_Y003) (derived from male mice) cells were cultured in Dulbecco's Modified Eagle Medium (Corning, 10-017-CV) supplied with 10% fetal bovine serum (Sigma-Aldrich, F0926) and 1% penicillin-streptomycin (Corning, 30-002-C). Cell line 005[48] (sex unspecified) was cultured in Dulbecco's Modified Eagle Medium/Nutrient Mixture F-12 (DMEM/F12) (Gibco, 11320033) supplemented with 2% B27 Supplement minus Vitamin A (Gibco, 12587010), 20 ng/mL epidermal growth factor (PeproTech, AF-100-15), 10 ng/mL fibroblast growth factor (PeproTech, 100-18B), and 1% penicillin-streptomycin (Corning, 30-002-C). Cell lines were not authenticated, routinely tested for mycoplasma contamination (abm Mycoplasma PCR Detection Kit, G238) and found negative.

METHOD DETAILS

Radiation therapy

For all RT experiments, a ^{137}Cs Mark 2 - Model 25 Irradiator (J.L. Shepherd & Associates) with turntable rotation was used. For animal RT studies, mice were anesthetized via 87.5 mg/kg ketamine and 12.5 mg/kg xylazine intraperitoneally and individually placed in an upright position in a 50mL Falcon tube without a tip to facilitate breathing. The tube was placed inside a custom-built 2cm thick lead shield that only exposes the head to radiation whilst shielding the body from the ears down.

Quantitative proteomics

Proteomes of cell lines were quantitatively mapped using multiplexed mass spectrometry (MS) by applying isobaric tandem mass tag (TMT) technology.[49,50] Lysis was performed in a buffer containing 75 mM NaCl, 50 mM HEPES (pH 8.5), 10 mM sodium pyrophosphate, 10 mM NaF, 10 mM β-glycerophosphate, 10 mM sodium orthovanadate, 10 mM phenylmethanesulfonylfluoride, Complete Protease Inhibitor EDTA-free

tablets (Roche), and 3% sodium dodecyl sulfate. Cells were lysed by passing them 10 times through a 21-gauge needle, and the lysates were prepared for analysis on the mass spectrometer essentially as described previously.[51,52] Briefly, reduction and thiol alkylation were followed by purifying the proteins using MeOH/CHCl3 precipitation. Protein digest was performed with Lys- C and trypsin, and peptides were labeled with TMT-16-plex reagents (Thermo Scientific)[53] and fractionated by basic pH reversed-phase chromatography.[51] Multiplexed quantitative proteomics was performed on an Orbitrap Lumos mass spectrometer (Thermo Scientific) using a Simultaneous Precursor Selection (SPS) based MS3 method.[49,50] MS2 spectra were assigned using a SEQUEST-based proteomics analysis platform[54] using the Uniprot mouse protein sequence database to which known contaminants such as trypsin were added. Based on the target-decoy database search strategy[55] and employing linear discriminant analysis and posterior error histogram sorting, peptide and protein assignments were filtered to a false discovery rate (FDR) of < 1%.[56] Peptides with sequences that were contained in more than one protein sequence from the UniProt database (RRID:SCR_004426) were assigned to the protein with most matching peptides.[56] TMT reporter ion intensities were extracted as that of the most intense ion within a 0.03 Th window around the predicted reporter ion intensities in the collected MS3 spectra. Only MS3 with an average signal-to-noise value larger than 20 per reporter ion as well as with an isolation specificity larger than 0.75 were considered for quantification. A two-step normalization of the protein TMT-intensities was performed by first normalizing the protein intensities over all acquired TMT channels for each protein based on the median average protein intensity calculated for all proteins. To correct for slight mixing errors of the peptide mixture from each sample, a median of the normalized intensities was calculated from all protein intensities in each TMT channel, and protein intensities were normalized to the median value of these median intensities.

RNA isolation and quantitative real-time PCR (q-PCR)

Cells were lysed, and RNA was extracted using the RNeasy mini kit (Qiagen, 74104), followed by cDNA synthesis using 5× All- In-One RT MasterMix kit (abm, G592). The expression of different genes was analyzed by quantitative real-time PCR using specific primers, with GAPDH and/or ACTB as an internal control (in triplicates) using a QuantStudio 3 PCR system (Applied Biosystems). The expression of various mouse genes analyzed in this study included: CD274, CD47, CD155, CD112, GAPDH, and ACTB. The sequence of all primers was obtained from the MGH primer bank (https://pga.mgh.harvard.edu/primerbank) and can be found in the key resources table.

TCGA-GBM survival analyses

TCGA-GBM[24] Kaplan-Meier plots were created with the SurvivalGenie[25] online tool using the cutp function (A cutpoint is estimated based on martingale residuals using the survMisc package to stratify patients into high and low groups). For gene set-based analyses, pre-defined cell sets provided by SurvivalGenie were used. Univariate Cox regression survival analysis showing the hazard ratio and 95% confidence intervals associated with two groups considered in the univariable analysis were created through SurvivalGenie. Graphs were further modified with Adobe Illustrator to improve visibility.

Cell transduction

Stably transduced fluorescent cell lines were generated by transducing CT-2A cells with mCherry, palm.tdTomato and/or H2B.mCerulean. Cells were incubated with lentivirus for 72 h, after which transfection media was removed, and fresh media was added. Successfully transduced cells were selected with FACS and expanded under standard conditions for no more than 20 passages.

Intracranial tumor injections

Adult mice were anesthetized using 2.5% isoflurane in 100% oxygen via a nose cone. A total of 5×10^4 CT-2A.m.Cherry, CT-2A.palm.tdTomato, CT-2A.H2B.mCerulean or CT-2A.palm.tdTomato.H2B.mCerulean cells were suspended in 2 μL of Opti-MEM (Gibco, 31985062). Using a Hamilton syringe (Sigma-Aldrich) and an automatic stereotaxic injector (Stoelting) with a flow rate of 0.2 μL/min, the cells were implanted into the left striatum of C57BL/6J (RRID:IMSR_JAX:000664) mice. For stereotactic implantation, three coordinates were selected relative to bregma: anterior-posterior (AP) = 0.5 mm, medial-lateral (ML) = −2.0 mm, and dorsal-ventral (DV) = −2.5 mm. All mice were 8–16 weeks of age and were randomly assigned to their treatment, with the experimenter being blind to the treatment groups.

Flow cytometry

Single-cell suspensions were prepared from the tumor-bearing hemisphere. Specifically, TME regions were isolated under the stereotactic microscope, followed by single-cell preparation. Cells were stained with antibodies Brilliant Violet 785 anti-mouse/human CD11b (Biolegend, #101243, RRID:AB_2561373), PerCP-eFluor 710 anti-mouse CD206 (Invitrogen, #46-2061-82, RRID:AB_2784688), Alexa Fluor 488 anti-mouse CD45 (Biolegend, #103121, RRID:AB_493532), Alexa Fluor 700 anti-mouse/human Ki-67 (Invitrogen, #56-5698-82, RRID:AB_2637480), APC anti-mouse CD274 (B7-H1, PD-L1) (Biolegend, #124311, RRID:AB_10612935), APC/Cyanine7 anti-mouse F4/80 (Biolegend, #123117, RRID:AB_893489), according to manufacturer's protocol. Non-specific binding of the immunoglobulin to the Fc receptors was blocked by incubating cells 10 min on ice in 0.5% BSA (Sigma Aldrich, A9576-50ML) in DPBS (Sigma Aldrich, D8537-500ML) with 2 mM EDTA (Invitrogen, 15575020) supplemented with TruStain fcX (anti-mouse Cd16/32, BioLegend, #101319, RRID:AB_1574973). For the flow cytometric analyses, ZombieUV (Biolegend, 423107) was used to identify live cells, and cells were stained with surface markers in FACS buffer (2% BSA in PBS) for 20 min on ice. For intracellular stain, eBioscience Foxp3/Transcription Factor Staining Buffer Set (Invitrogen, #00-5523-00) was used according to manufacturer's protocol). Live cells for *in vivo* experiments were sorted using 4 Laser BD FACSAria II Cell Sorter (BD Biosciences). Cells were

analyzed on Aria II (BD Biosciences) or Fortessa X-20 (BD Biosciences), and data analysis was performed on FlowJo (v10.8.1, RRID:SCR_008520).

Single cell RNA-sequencing dataset analysis

Gene-cell count and cell annotation matrices were procured from the Brain Immune Atlas (www.brainimmuneatlas.org). This atlas includes data from GL261 tumor-bearing mice, newly diagnosed GBM patients, and individuals with recurrent GBM samples.[21] Data preprocessing and analysis were conducted using the Seurat v4 R package.[57] The Seurat workflow was followed, with default quantitative parameters, excluding low-quality cells. Gene expression values underwent global-scaling normalization ("LogNormalize" method). Top 2000 variable genes were identified through the "FindVariableFeature" function with variance stabilizing transformation ("vst"). Gene expression values were scaled across cells using the "scaleData" function. Principal component analysis (PCA) was used for dimensionality reduction. Clustering utilized the "FindNeighbors" and "FindClusters" functions. Visualization of clustering results was achieved through Uniform Manifold Approximation and Projection (UMAP). Cell types were defined based on the original cell annotation matrices.[21] Expression levels of genes of interest were examined using Seurat's "VlnPlot," "FeaturePlot," and "AverageExpression" functions. Calculation of the proportion of cells per cluster expressing genes of interest (normalized counts >0) was also performed.

Immunohistochemistry

For *in vivo* sections, the brains were removed, kept in 4% PFA (EMS, 15714) overnight and 30% sucrose for 48 h, and then cryosectioned at 40-μm thickness. Slides were then mounted with Antifade Mounting Medium with DAPI (Vector Labs, H-1200-10). Fluorescence microscopy images were acquired on a Keyence (Itasca) microscope and processed using ImageJ2 v2.3.0 (RRID:SCR_003070).

For *in vitro* EV uptake experiments, bone marrow-derived macrophages (BMDM) were exposed to EVs for 24 h, washed with PBS for three times, and fixed using 100% ice-cold methanol for 10 min. After fixation, cells were rinsed twice in PBS for 5 min each. Blocking was achieved by using 5% BSA and 0.1% Tween 20 (Sigma Aldrich, P1379-25ML) in PBS (PBS-T) for 4 h. Cells were then incubated with the anti-mouse F4/80 Antibody conjugated to Alexa Fluor 488 (BioLegend, #123119, RRID:AB_893491) for 1h at room temperature. Cells were rinsed three times in PBS-T for 5 min each. Coverslips were transferred to microscope slides (Fisherbrand) on a droplet of mounting medium containing DAPI (Vectashield; Vector Labs, H-1200-10). Fluorescence microscopy images were acquired on a Keyence (Itasca) and LSM710 Laser Scanning Confocal (Zeiss) microscope and processed using ImageJ2 v2.3.0 (RRID:SCR_003070).

Bone marrow-derived macrophage isolation

BMDM (bone marrow-derived macrophages) were isolated from both femurs and tibias of 8-week-old C57BL/6J (RRID:IMSR_JAX:000664) mice as previously described.[58] In brief, mice were euthanized, soaked in 70% ethanol, and attached tissues from femurs and tibias were removed before bone marrow was flushed out. The bone marrow suspension was filtered through a 100 μm cell strainer and erythrocytes were removed with 1X RBC Lysis Buffer (eBioscience, 50-112-9751). Pellets were resuspended in Dulbecco's Modified Eagle Medium (Corning, 10-017-CV) supplied with 10% fetal bovine serum (Sigma-Aldrich, F0926), 1% penicillin-streptomycin (Corning, 30-002-C), and 10 ng/ml recombinant mouse M-CSF (Biolegend, 576404). Cells were cultured in 6-well plates for 7 days. Attached macrophages were washed with PBS for 3 times and either treated or detached for downstream applications.

EV isolation

EVs were isolated by size exclusion chromatography (SEC) using Izon qEVoriginal/70 nm columns (IZON, SP1) as follows: On day 1, cells were seeded in 150 mm dishes. For cells growing in media supplemented with FBS, the culture medium was exchanged with fresh medium supplemented with 10% ultracentrifugation EV-depleted FBS on day 2. Ultracentrifugation EV-depleted FBS was obtained by overnight centrifugation of FBS (Sigma-Aldrich, F0926) at 100,000g, 4°C followed by double filtration with 0.22mm low binding filters. To isolate irEVs (EVs derived from cells exposed to ionizing radiation), cells were irradiated with 5 Gy immediately after changing the media. On day 4, conditioned media was collected and centrifuged at 300g for 5 min. The supernatant was transferred to a UFC9100 Amicon Ultra-15 Centrifugal filter (100 kDa) (Millipore, UFC900396) and centrifuged at 4,500g for 20 min. The concentrated sample (500 μL) was added to the Izon column after priming it with 10 mL 1X PBS. Then, 15 mL PBS was added, and fractions were collected using an IZON automatic fraction collector. For the transfer of EVs, fractions 7–10 were concentrated using AmiconUltra-0.5 Centrifugal (30 kDa) (Millipore, UFC503024) to reduce the volume from 2.5 mL to 30–80 μL. For all functional analyses of EVs, each step was performed in a sterile manner.

EV quantification

EV concentration and size were analyzed using the NanoSight LM10 instrument (Malvern) equipped with an AVT MARLIN F-033B IRF camera (Allied Vision Technologies) and NTA 3.1 Build 3.1.46 software.

All nanoparticle tracking analyses were conducted with consistent experiment settings, including Camera Level set at 12 and Detection Threshold set at 4. The particles were measured for a duration of 30 s, and to ensure optimal results, the EV concentrations were adjusted to achieve approximately 50 EVs per field of view. Each sample was imaged in a minimum of 5 technical replicates.

Western blot

Proteins were isolated by resuspending cell and EV pellets in RIPA buffer (Boston-Bioproducts, BP-115) containing Halt Protease and Phosphatase Inhibitor Cocktail (100X) (Thermo-Fisher, 78440) and sonicated. Next, proteins were quantified using Pierce Bradford Plus Protein Assay Reagent (Thermo Scientific, 23238). Then, 20μg of protein was loaded on a 4–12% Bis-Tris NuPage gel (Invitrogen, NP0322BOX) using NuPage MES SDS Running Buffer (Invitrogen, NP0002) followed by electrophoresis. Proteins were then transferred to nitrocellulose membranes using NuPage Transfer Buffer (Invitrogen, NP00061). The membranes were incubated overnight at 4°C with primary antibodies in 2.5% nonfat milk powder in PBS containing 0.1% Tween 20 (Sigma Aldrich, P1379-25ML). The primary antibodies used in this study were β-actin (Cell Signaling Technology, 4967), Alix (Santa Cruz Biotechnology, sc-53538), CD81 (Cell Signaling Technology, 56039S), and CD9 (Cell Signaling Technology, 98327S). Next, membranes were probed with secondary anti-rabbit (Cell Signaling Technology, 7074) or anti-mouse (Cell Signaling Technology, 7076) HRP conjugated for 1 h at room temperature. Finally, proteins were visualized using SuperSignal West Pico Plus Chemiluminescent Substrate (Thermo Fisher).

EV treatment

BMDMs were treated with 1×10^{10} EVs mL^{-1} in Dulbecco's Modified Eagle Medium supplied with 10% ultracentrifugation EV-depleted FBS daily for 2 days before downstream analyses 24h after last EV treatment.

Cytokine array

EV-treated BMDMs were washed with PBS 3 three times, and Dulbecco's Modified Eagle Medium (Corning, 10-017-CV) was added. The supernatant was isolated from culture conditions after 24h, centrifuged at 500g for 5 min to remove cellular debris, and transferred to a tube for storage at −80°C until use. The cytokine array was performed using the Proteome Profiler Mouse XL Cytokine Array (R&D Systems, ARY028s) according to the manufacturer's protocol.

Phagocytosis assay

BMDMs were treated with EVs as described above, washed with PBS, and detached by adding 5mM EDTA for 20 min at 4°C. BMDMs were centrifuged at 500g for 3min and labeled with CellTrace Violet (Invitrogen, C34557) according to the manufacturer's protocol. Cancer cells (CT-2A or 005) were labeled with pHrodo Red Intracellular pH Indicator Dye (Invitrogen, P35372) according to the manufacturer's protocol. BMDMs and cancer cells were co-cultured in a 96-well low adherent U-bottom plate (Corning) in a ratio of 1:4 for 4 h at 37°C. For some conditions, anti-CD47 antibody (10 μg/mL) (MIAP410, Bio x Cell, BE0283, RRID:AB_2687806) was added at the beginning of the co-culture. Cells were collected on ice, washed 2 times with cold Live Cell Imaging Solution (Thermo Fisher, A14291DJ), and fixed with a solution of 4% paraformaldehyde before analysis. Phagocytosis was analyzed using a Fortessa X-20 cell sorter (BD Biosciences) and calculated as the percentage of pHrodo Red+ cells within the total CellTrace Violet+ BMDM population.

QUANTIFICATION AND STATISTICAL ANALYSIS

GraphPad Prism (v.10.0.0, RRID:SCR_002798) was used for statistical analysis of all data. GraphPad Prism (v.10.0.0, RRID:SCR_002798) and Adobe Illustrator 2022 (RRID:SCR_010279) were used to create the graphs and figures. The findings are displayed as the average ± standard deviation (SD) or standard error of the mean (SEM). To assess the normality of the data distribution, a Shapiro-Wilks test was employed. For groups with a normal distribution, Student's t-test or ANOVA was used for comparison. For groups with a non-normal distribution, the Mann-Whitney test was employed. Results with p values less than 0.05 (*$p < 0.05$; **$p < 0.01$; ***$p < 0.001$) were considered statistically significant.